Depth-resolved cathodoluminescence spectroscopy study of defects in Sr Ti O 3

Jun Zhang, S. Walsh, C. Brooks, D. G. Schlom, and L. J. Brillson

Depth-resolved cathodoluminescence spectroscopy study of defects in SrTiO₃

Jun Zhang
Department of Physics, Ohio State University, Columbus, Ohio 43210

S. Walsh
Department of Electrical and Computer Engineering and Department of Physics, Ohio State University, Columbus, Ohio 43210

C. Brooks and D. G. Schlom
Department of Materials Science and Engineering, Pennsylvania State University, University Park, Pennsylvania 16802

L. J. Brillson[a)]
Department of Electrical and Computer Engineering and Department of Physics, Ohio State University, Columbus, Ohio 43210

The authors report a depth-resolved cathodoluminescence spectroscopy study of defects and their distributions in SrTiO₃ single crystals and epilayers. In SrTiO₃ single crystals, the dominant defects are oxygen vacancies that locate mainly near the free surface, while Ti interstitials locate further into the bulk. Vacuum annealing increases the density of oxygen vacancies at SrTiO₃ surfaces but reduces the density of Ti interstitials located deeper. In epilayers, the density and distribution of the defects depend on the film thickness and stoichiometry. The results reveal a strong dependence of SrTiO₃ native point defects and their depth distributions on epitaxial growth and process conditions. © 2008 American Vacuum Society. [DOI: 10.1116/1.2918315]

I. INTRODUCTION

Strontium titanate (SrTiO₃) is one of the most widely used electronic materials, with applications ranging from a high dielectric constant paraelectric[1] to a ferroelectric induced by epitaxial strain[2] to a semiconductor or even to a superconductor if suitably doped.[3,4] It has wide applications in tunable dielectric devices, in dynamic random access memory, and in high permittivity gate oxides for metal-oxide-semiconductor transistors. Furthermore, it is an excellent substrate for many perovskite oxides. The broad range of physical properties and applications of SrTiO₃ make it very important to investigate its electronic band structure and defects. This is especially the case since electronic defects in such perovskites limit multifunctional material efficiency and loss, and significantly vary with material growth and processing conditions. Therefore, before growing oxide thin films or fabricating devices on SrTiO₃ single crystal substrates, it would be very important to know what kind of defects the substrates have and how the distributions of the defects can be changed by thermal processing during film growth and device fabrication. It would also be interesting to understand how the defects and their distribution in SrTiO₃ thin films differ from those in the single crystal substrates.

In order to study the defects and other electronic states in SrTiO₃, we use cathodoluminescence spectroscopy (CLS), a powerful technique in directly detecting the band-to-band transitions and defect optical transitions. Depth-resolved CLS (DRCLS), in which the incident electron beam penetration depth varies with beam energy, can be used to probe the defects at surfaces and interfaces of ultrathin films and bulk materials, as well as to provide unique information about the defect distributions.[5–9] Here, we report direct measurements of defects and their distribution in SrTiO₃ single crystals and epilayers by using the DRCLS technique. We find that the main deep level defects in SrTiO₃ are titanium interstitials (Ti$_i$) and oxygen vacancies (V_O), and their distributions are strongly dependent on material growth and processing.

The identification of native point defects in SrTiO₃ rests on a similar identification for defects in TiO₂. This is because the valence band of both SrTiO₃ and TiO₂ are derived entirely from O^{2-}-$2p$ states and the lowest unoccupied conduction bands of both are derived from Ti^{3+}-$3d$ states. Very similar cathodoluminescence (CL) emission features have been observed in SrTiO₃ and TiO₂.[10] In TiO₂, emissions from Ti$_i$ occur at around 1.5 eV.[11–13] Emission peaks at 2.19 and 2.6 eV are attributed to V_O and oxygen vacancy complexes (V_O complexes),[14–16] respectively, and peaks at ~2.9 eV are due to self-trapped excitons.[10,16] The V_O complexes can be V_O with surrounding titanate groups,[14] or V_O with trapped charges, forming F centers.[15]

II. EXPERIMENT

The SrTiO₃ samples we studied are commercially available single crystals and thin films grown by molecular beam epitaxy (MBE). SrTiO₃ films were epitaxially grown on SrTiO₃ substrates under 5×10^{-7} Torr O₂ with 10% O₃ at a substrate temperature of 650 °C. The SrTiO₃ single crystal substrates were chemically cleaned by using standard sub-

---

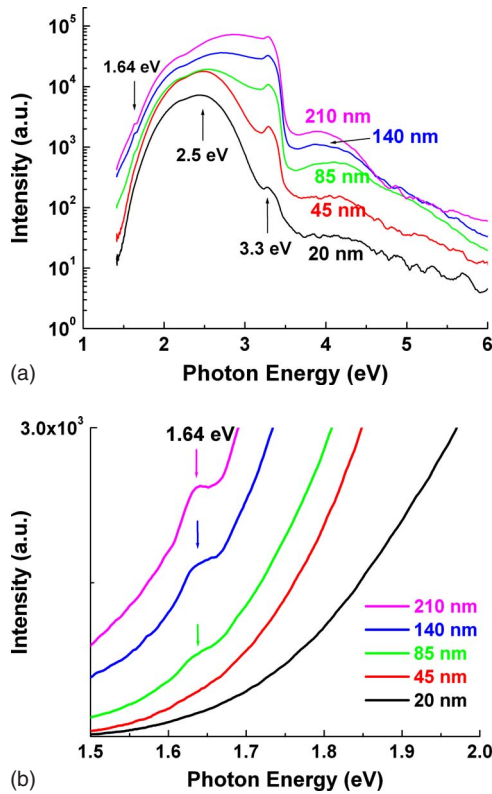a)Electronic mail: brillson.1@osu.edu

FIG. 1. CL spectra of an unprocessed SrTiO$_3$ single crystal substrate. (a) Full spectral range and (b) low energy spectral region.

FIG. 2. CL spectra of the unprocessed SrTiO$_3$ single crystal substrate for the penetration depths of (a) 20 nm and (b) 210 nm. Black curves: original data; red curves: fitted data; and blue curves: decomposed peaks.

strate pretreatment method. No further processing was made for the unprocessed substrates and the processed substrates were further annealed at the thin film growth condition for 100 min. By comparing the unprocessed and processed SrTiO$_3$ substrates, we can learn how the distribution of defects in SrTiO$_3$ substrates changes after thin films are grown on them. DRCLS measurements were performed in an ultra-high vacuum chamber with samples cooled with a helium cryotip to ∼42 K for all samples. Depth-dependent CL spectra were collected with the incident electron beam current held constant at 2 mA and the beam voltage varied from 1 to 5 kV so that the beam power increases with increasing beam voltage. Monte Carlo simulations for SrTiO$_3$ established a relationship between the beam voltage and the maximum excitation depth. As beam voltage increases from 1 to 5 kV, the excitation depth increases from 20 to 210 nm. In this article, we present CL spectra denoted by their excitation depths instead of their beam voltages.

III. RESULTS

A. Unprocessed SrTiO$_3$ substrates

The CL spectra of an unprocessed SrTiO$_3$ single crystal substrate are shown in Fig. 1(a). The crystal shows a strong feature at 3.3 eV, which is the SrTiO$_3$ bandgap emission, a broad peak between 2 and 3 eV, and a weak feature at 1.64 eV, which is attributed to Ti$_i$. The feature at 1.64 eV more clearly appears in Fig. 1(b), which magnifies the low energy range of the CL spectra. Interestingly, the 1.64 eV
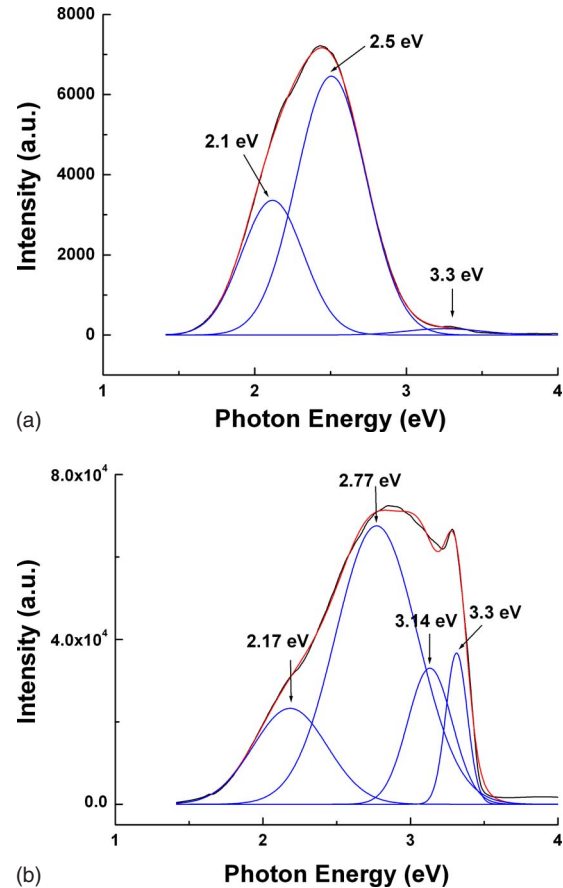
feature is only observed for penetration depths deeper than 45 nm and becomes stronger as the penetration depth increases. This suggests that more Ti$_i$ are located in the bulk rather than at the surface of the SrTiO$_3$ single crystals. Features above the 3.3 eV SrTiO$_3$ bandgap are due to higher energy transitions between O 2p and Ti 3d levels[17,18] as well as parasitic emission due to electrons incident on the SiO$_2$ collection lens. Only features of up to 3.3 eV will be discussed.

Evidently, there are multiple peaks in the CL spectra between 2 and 3 eV, which we deconvolved for photon energies below 4 eV. For the penetration depths of 20 and 45 nm, the broad peak between 2 and 3 eV can be deconvolved into two peaks, one at 2.1 eV and another at 2.5 eV. Figure 2(a) shows the decomposition result for the penetration depth of 20 nm. The 2.1 eV peak is ascribed to V_O and the 2.5 eV peak is related to V_O complexes. As the environment of V_O changes, the DRCLS peak related to V_O complexes shifts. For the penetration depths beyond 45 nm, the broad peak can be decomposed into three peaks, with an additional peak at 3.14 eV whose origin is not yet clear. As an example, Fig. 2(b) shows the deconvolution result for the penetration depth of 210 nm. Compared to the peaks in Fig. 2(a), the V_O peak slightly shifts to higher energy but the V_O
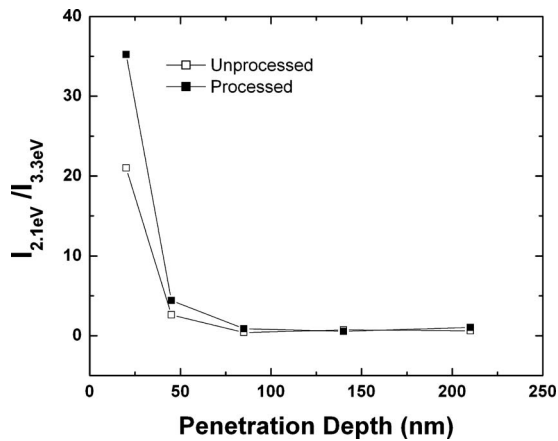
FIG. 3. Intensity ratio of the 2.1 eV peak to the 3.3 eV peak as a function of excitation depth for the unprocessed (●) and processed (□) substrates. Both strongly decrease from 25 to 100 nm.

FIG. 4. CL spectra of the processed $SrTiO_3$ single crystal substrate. (a) Full spectra and (b) spectra in low energy range.

complex peak significantly shifts from 2.5 to 2.77 eV, indicating different environments of V_O at the surface and in the bulk.

Moreover, the intensity of the 2.1 eV V_O peak changes with the penetration depth. The intensity ratio of the 2.1 eV peak to the 3.3 eV bandgap emission peak I (2.1 eV)/I (3.3 eV) is plotted in Fig. 3 as a function of the penetration depth. The ratio dramatically decreases as the penetration depth increases from 20 to 85 nm, then remains almost constant as the penetration depth further increases to 210 nm. The result clearly indicates that most of the V_O defects locate near the surface rather than in the bulk of $SrTiO_3$ single crystals, in contrast with the distribution of Ti_i, which locate mainly in the bulk of $SrTiO_3$.

B. Vacuum-annealed $SrTiO_3$ substrates

The effect of vacuum annealing on the intensity and distribution of defects in $SrTiO_3$ single crystals was studied since similar treatments are often used in preparation for MBE growth of epitaxial perovskite overlayers. Figure 4(a) shows the CL spectra of the *same* vacuum-annealed $SrTiO_3$ substrate examined before annealing. The spectra appear similar to those of the unprocessed substrate but detailed analysis showed changes in the Ti_i and V_O. As shown by the CL spectra at low energy range in Fig. 4(b), the Ti_i-related 1.64 eV peak is now only observed for the penetration depths of 140 nm and deeper. As mentioned before and shown in Fig. 1(b), the 1.64 eV peak for the unprocessed substrate initially appears for shallower penetration depths of 85 nm. Moreover, the 1.64 eV peak in the processed substrate is weaker than that in the unprocessed one for the same penetration depth. Therefore, vacuum annealing reduces the density of the Ti_i. As with the unprocessed substrate, the CL spectra below 4 eV of the processed substrate were deconvolved, and I (2.1 eV)/I (3.3 eV) is plotted in Fig. 3. For the penetration depth of 20 nm, the relative intensity of the 2.1 eV peak of the processed substrate is nearly a factor of 2 higher than that of the unprocessed substrate, but the differ-
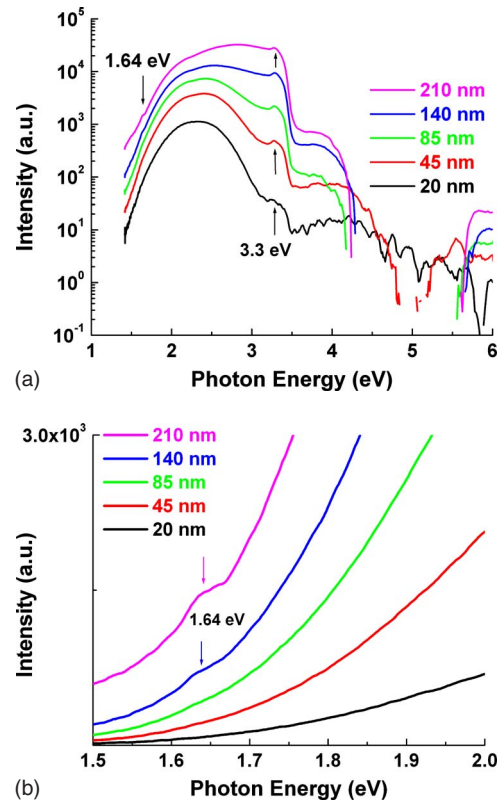
ence in intensity decreases very fast as the penetration depth increases below the top 50–80 nm. Thus, vacuum annealing increases the density of V_O in $SrTiO_3$ single crystals but the effect is limited to depths 50–80 nm below the surface.

One would expect the densities of both V_O and Ti_i to increase upon vacuum annealing. However, in our $SrTiO_3$ single crystal samples, V_O and Ti_i are located at different depths; V_O are mainly in the near-surface region, within the top 85 nm, but Ti_i locate in the bulk of the crystals, deeper than 85 nm. Due to their spatial separation, the annealing effects on the two types of defects may not be correlated. The vacuum annealing increases the density of V_O near the surface and reduces the density of Ti_i that locate deeper in the bulk. The latter effect could be due to thermal diffusion and recovery of defects during annealing since short-range migration pathways exist for Ti interstitials in $SrTiO_3$.[19]

C. $SrTiO_3$ epilayers on $SrTiO_3$ substrates

Figure 5 shows the CL spectra of $SrTiO_3$ epilayers grown on the $SrTiO_3$ substrates. For the 50 nm thick epilayer [Fig. 5(a)], there are two peaks in the low energy range at 1.57 and 1.7 eV, respectively, both of which are associated with Ti_i defects.[11,14] These peaks are present for all penetration depths, indicating that they are present in the epilayer. The peaks between 2.0 and 2.6 eV are related to V_O and V_O complexes. Since these peaks are evident only for penetration depths beyond the 50 nm epilayer thickness, they probably come from the V_O-related defects locating at the epilayer-
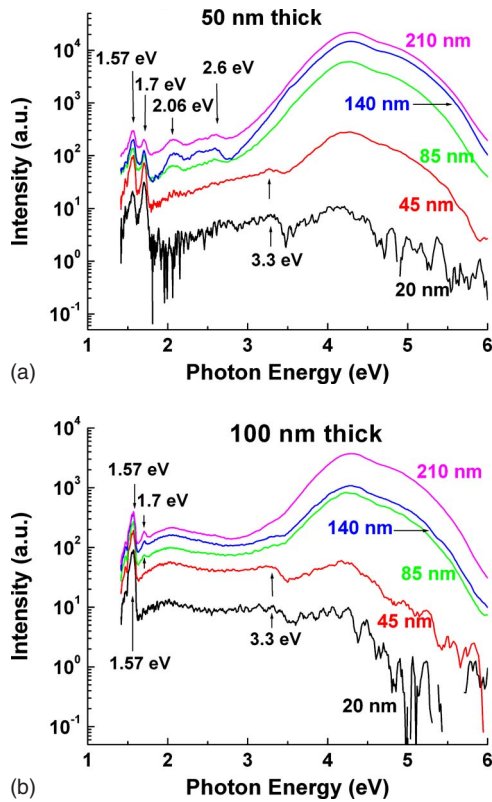
FIG. 5. CL spectra of (a) 50 nm thick and (b) 100 nm thick SrTiO$_3$ epilayers.

substrate interface or in the SrTiO$_3$ substrate. Therefore, the SrTiO$_3$ epilayer contains considerable Ti$_i$ but very few V_O. In the case of the 100 nm thick SrTiO$_3$ epilayer [Fig. 5(b)], only the 1.57 eV peak appears for all penetration depths, suggesting its epilayer origin. The 1.7 eV peak is much weaker than the 1.57 eV peak, and is evident only for penetration depths of 85 nm and beyond, suggesting that it is

associated with Ti$_i$ that is located at the interface or in part of the epilayer near the interface. Furthermore, the peaks between 2.0 and 2.6 eV that are observed for the 50 nm thick epilayer are absent for all penetration depths for the 100 nm thick epilayer. So, for the thicker epilayer, both the epilayer and the interface contain very few V_O.

D. Sr$_x$TiO$_3$ epilayers on SrTiO$_3$ substrates

The density and distribution of the defects in SrTiO$_3$ epilayers also strongly depend on the stoichiometry. CL spectra of Sr$_x$TiO$_3$ epilayers with Sr composition x equal to 0.8, 1.0, and 1.2 are shown in Fig. 6. All epilayers show similar bandgap emissions at 3.3 eV but different CL features related to defects. For the Sr-deficient epilayer with $x=0.8$, the Ti$_i$-related 1.5 eV peak can be clearly seen at the penetration depth of 210 nm. However, this peak is barely visible in the stoichiometric epilayer with $x=1.0$ and is completely absent in the Sr-rich epilayer with $x=1.2$. With increasing x, the V_O-related 2.0 eV peak becomes stronger. This trend is more clearly shown in Fig. 7, in which the intensity ratio of I $(2.0 \text{ eV})/I$ (3.3 eV) at the 210 nm penetration depth is plotted as a function of the Sr composition x in the Sr$_x$TiO$_3$ epilayers. The higher the Sr composition is, the more V_O defects are in the epilayers and the stronger the 2.0 eV peak is. The epilayer with $x=1.2$, which is the richest in Sr, has the strongest 2.0 eV peak, indicating the highest density of V_O.

IV. DISCUSSION

The results presented here show that electrically active native point defects such as Ti$_i$, V_O, and V_O complexes are commonly present in the SrTiO$_3$ substrates and epilayer films. The DRCLS features show that these defects vary in concentration as a function of depth below the free surface. V_O defects exist with relatively high concentration near free
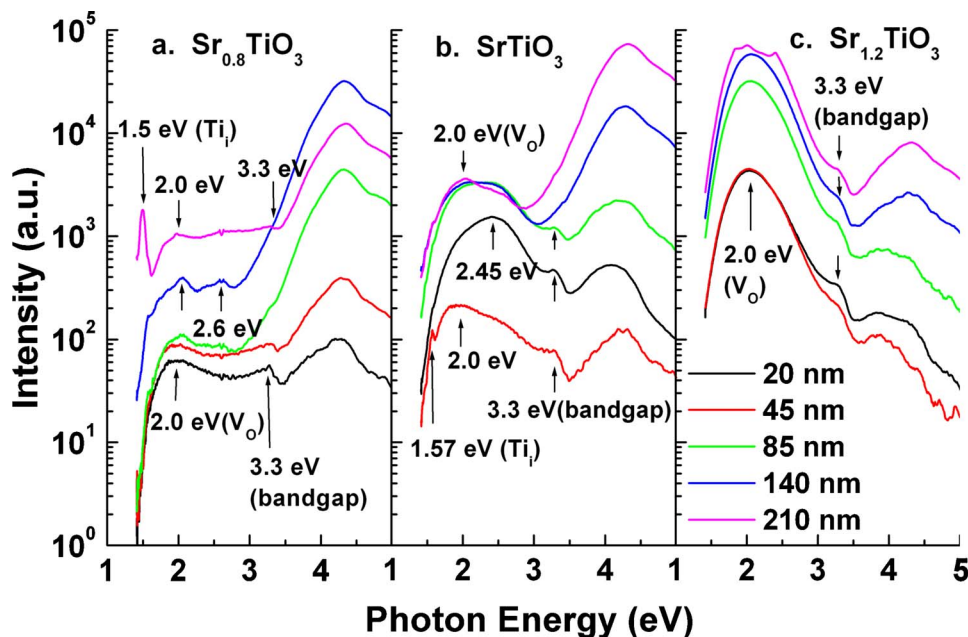

FIG. 6. CL spectra of Sr$_x$TiO$_3$ epilayers. (a) $x=0.8$, (b) $x=1.0$, and (c) $x=1.2$.
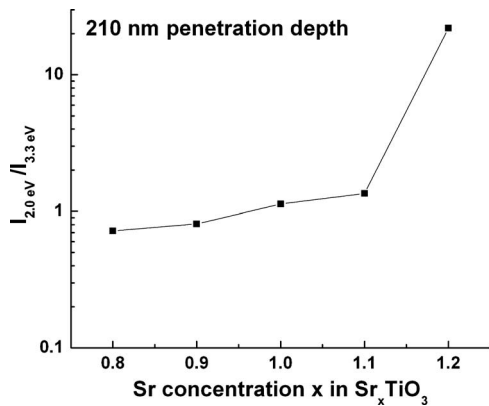
FIG. 7. Intensity ratio of the 2.0 eV peak to the 3.3 eV bandgap peak at the 210 nm penetration depth as a function of the Sr composition x in the Sr_xTiO_3 epilayers.

surfaces of $SrTiO_3$ substrates and appear to be considerably reduced in homoepitaxial overlayers, more so for the 100 nm versus the 50 nm films. These lower V_O concentrations may be due to the ozone MBE growth technique employed in the film growth, designed to enhance oxygen incorporation. The increase in DRCLS V_O emission for depths at and beyond the interface underscores their substrate rather than epilayer position. On the other hand, the DRCLS emissions related to Ti_i appear for depths starting at 85 nm for the unprocessed and 140 nm for the processed $SrTiO_3$ substrates. The lowering of the density of Ti_i in the region between 85 and 140 nm may be due to a diffusion process promoted by the annealing.

It should be noted that the 1.6 eV peak feature ascribed to Ti_i is not likely due to impurities. A review of literature shows that the main impurities in $SrTiO_3$ are Fe and Al but the energy levels of these defects are not consistent with the 1.6 eV photon energy of the defect emission of our $SrTiO_3$ substrates.[20] Moreover, an Fe impurity usually gives rise to multiple emissions,[20–22] in contrast to the single 1.6 eV emission of our samples. In addition, we have carried out second ion mass spectroscopy (SIMS) measurements on our $SrTiO_3$ substrates. SIMS results indicate only the presence of trace Fe and Al within a few nanometers of the surface, most likely due to surface contamination, but no Fe, Al, and other impurities in the substrate.[23] Therefore, we ascribe the 1.6 eV peak feature to intrinsic defects rather than impurities.

The behavior of these native point defects is significant since their electrical behavior could play a role in many perovskite physical phenomena. The use of $SrTiO_3$ and related perovskites have led to the observation of charge modulation layers,[24] quasi-two-dimensional electron gases,[25] superconducting interfaces at the junction between two insulators,[26] and strain-induced ferroelectric behavior.[27,28] In the case of highly conducting interface layers, the contribution of native point defects remains controversial.[29]

The DRCLS results shown in Fig. 6 reveal dramatic differences between the Sr_xTiO_3 epilayers of varying composition. In particular, the ratio of the V_O to near band edge

emissions varies by over an order of magnitude between x =0.8 and 1.2. The V_O appears to increase with increasing Sr content. This may be related to formation of a partial $Sr_{n+1}Ti_nO_{3n+1}$ Ruddleson-Popper phase during growth without sufficient oxygen to maintain stoichiometry. Moreover, the defect peak ascribed to Ti_i varies with stoichiometry as well—another indication that this feature is not impurity related. This defect appears only for the Sr-deficient epilayers. Such a direct relationship between CL features and stoichiometry could be utilized to guide growth of stoichiometric $SrTiO_3$ as well as other complex oxides.

V. CONCLUSIONS

In summary, we have studied defects and their distributions in $SrTiO_3$ single crystals and epilayers using DRCLS. In $SrTiO_3$ single crystals, oxygen vacancies are the main defects and locate mainly at surface, while Ti interstitials are the minor defects and locate in the bulk. Vacuum annealing increases the density of oxygen vacancy near the surface and reduces the density of Ti interstitials in bulk. In $SrTiO_3$ epilayers, both intrinsic and interface-specific defects are observed, and density and distribution of defects strongly depend on the thickness and stoichiometry. Our results reveal strong dependence of defects and their distributions in $SrTiO_3$ on material growth and processing, and suggest that DRCLS may serve to guide growth of stoichiometric and low-defect complex oxide thin films.

[1]H. M. Christen, J. Mannhart, E. J. Williams, and Ch. Gerber, Phys. Rev. B **49**, 12095 (1994).
[2]J. H. Haeni, P. Irvin, W. Chang, R. Uecker, P. Reiche, Y. L. Li, S. Choudhury, W. Tian *et al.*, Nature (London) **430**, 758 (2004).
[3]C. S. Koonce, M. L. Cohen, J. F. Schooley, W. R. Hosler, and E. R. Pfeiffer, Phys. Rev. **163**, 380 (1967).
[4]G. Binnig, A. Baratoff, H. E. Hoenig, and J. G. Bednorz, Phys. Rev. Lett. **45**, 1352 (1980).
[5]R. Viturro, M. L. Slade, and L. J. Brillson, Phys. Rev. Lett. **57**, 487 (1986).
[6]L. J. Brillson and R. E. Viturro, Scanning Microsc. **2**, 789 (1988).
[7]L. J. Brillson, J. Vac. Sci. Technol. B **19**, 1762 (2001).
[8]L. J. Brillson, J. Vac. Sci. Technol. A **25**, 943 (2007).
[9]H. L. Mosbacker, C. Zgrabik, M. J. Hetzer, A. Swain, D. C. Look, G. Cantwell, J. Zhang, J. J. Song *et al.*, Appl. Phys. Lett. **91**, 072102 (2007).
[10]H. Ihrig, J. H. T. Hengst, and M. Klerk, Z. Phys. B: Condens. Matter **40**, 301 (1981).
[11]R. Plugaru, A. Cremades, and J. Piqueras, J. Phys.: Condens. Matter **16**, S261 (2004).
[12]A. K. Ghosh, F. G. Wakim, and R. R. Addiss, Phys. Rev. **184**, 979 (1969).
[13]R. Sanjinés, H. Tang, H. Berger, F. Gozzo, G. Margaritondo, and F. Lévy, J. Appl. Phys. **75**, 2945 (1994).
[14]D. Maestre, A. Cremades, and J. Piqueras, Nanotechnology **17**, 1584 (2006).
[15]Y. Lei, L. D. Zhang, G. W. Meng, G. H. Li, X. Y. Zhang, C. H. Laing, W. Chen, and S. X. Wang, Appl. Phys. Lett. **78**, 1125 (2001).
[16]J.-M. Wu, H. C. Shih, W.-T. Wu, Y.-K. Tseng, and I.-C. Chen, J. Cryst. Growth **281**, 384 (2005).
[17]M. Cardona, Phys. Rev. **140**, A651 (1965).
[18]K. van Benthem, C. Elsässer, and R. H. French, J. Appl. Phys. **90**, 6156 (2001).
[19]W. J. Weber, W. Jiang, S. Thevuthasan, R. E. Williford, A. Meldrum, and L. A. Boatner, *Defects and Surface-induced Effects in Advanced Perovskites*, edited by G. Borstel, A. Krumins, and D. Millers (Springer, New York, 2000), pp. 317–328.
[20]F. J. Morin and J. R. Oliver, Phys. Rev. B **8**, 5847 (1973).

[21]W. A. Feil and B. W. Wessels, J. Appl. Phys. **74**, 3927 (1993).

[22]J. Zhang, S. Walsh, and L. J. Brillson (unpublished).

[23]J. Zhang, G. Sollenberger, R. Adur, C. Brooks, D. G. Schlom, and L. J. Brillson (unpublished).

[24]A. Ohtomo, D. A. Muller, J. L. Grazul, and H. Y. Hwang, Nature (London) **419**, 378 (2002).

[25]S. Thiel, G. Hammerl, A. Schmehl, C. W. Schneider, and J. Mannhart, Science **313**, 1942 (2006).

[26]N. Reyren, S. Thiel, A. D. Caviglia, L. Fitting Kourkoutis, G. Hammerl, C. Richter, C. W. Schneider, T. Kopp *et al.*, Science **317**, 196 (2007).

[27]J. Haeni, P. Irvin, W. Chang, R. Uecker, P. Reiche, Y. L. Li, S. Choudhury, W. Tian *et al.*, Nature (London) **430**, 758 (2004).

[28]K. J. Choi *et al.*, Science **306**, 1005 (2004).

[29]W. Siemons, G. Koster, H. Yamamoto, W. A. Harrison, G. Lucovsky, T. H. Geballe, D. H. A. Blank, and M. R. Beasley, Phys. Rev. Lett. **98**, 196802 (2007).